Biochimica et Biophysica Acta 1847 (2015) 46–54

Contents lists available at ScienceDirect

Biochimica et Biophysica Acta

journal homepage: www.elsevier.com/locate/bbabio

Review

Reaction dynamics and proton coupled electron transfer: Studies of tyrosine-based charge transfer in natural and biomimetic systems ☆

Bridgette A. Barry *

School of Chemistry and Biochemistry, Georgia Institute of Technology, Atlanta, GA 30332, USA
Petit Institute for Bioengineering and Biosciences, Georgia Institute of Technology, Atlanta, GA 30332, USA

ARTICLE INFO

Article history:
Received 9 May 2014
Received in revised form 27 August 2014
Accepted 10 September 2014
Available online 28 September 2014

Keywords:
Ribonucleotide reductase
Azurin
Photosystem II
EPR spectroscopy
RIFT-IR spectroscopy
DNA synthesis

ABSTRACT

In bioenergetic reactions, electrons are transferred long distances via a hopping mechanism. In photosynthesis and DNA synthesis, the aromatic amino acid residue, tyrosine, functions as an intermediate that is transiently oxidized and reduced during long distance electron transfer. At physiological pH values, oxidation of tyrosine is associated with a deprotonation of the phenolic oxygen, giving rise to a proton coupled electron transfer (PCET) reaction. Tyrosine-based PCET reactions are important in photosystem II, which carries out the light-induced oxidation of water, and in ribonucleotide reductase, which reduces ribonucleotides to form deoxynucleotides. Photosystem II contains two redox-active tyrosines, YD (Y160 in the D2 polypeptide) and YZ (Y161 in the D1 polypeptide). YD forms a light-induced stable radical, while YZ functions as an essential charge relay, oxidizing the catalytic Mn_4CaO_5 cluster on each of four photo-oxidation reactions. In *Escherichia coli* class 1a RNR, the β2 subunit contains the radical initiator, Y122O•, which is reversibly reduced and oxidized in long range electron transfer with the α2 subunit. In the isolated *E. coli* β2 subunit, Y122O• is a stable radical, but Y122O• is activated for rapid PCET in an α2β2 substrate/effector complex. Recent results concerning the structure and function of YD, YZ, and Y122 are reviewed here. Comparison is made to recent results derived from bioengineered proteins and biomimetic compounds, in which tyrosine-based charge transfer mechanisms have been investigated. This article is part of a Special Issue entitled: Vibrational spectroscopies and bioenergetic systems.

1. Introduction

In photosynthesis and respiration, electrons must be transferred long distances across a membrane. Electron transfer (ET) reactions are mediated by tunneling with rates that decrease exponentially with distance [1]. To accelerate bioenergetic ET reactions and make them biologically useful, redox-active cofactors are embedded into the protein matrix [2]. These redox-active cofactors are transiently oxidized and reduced and define a radical transport pathway. The aromatic amino acid, tyrosine, serves as such a redox-active cofactor in photosynthesis and DNA synthesis (reviewed in ref. [3]). Tyrosine charge transfer has also been proposed to play important roles in other metabolic processes, including galactose oxidation [4], prostaglandin synthesis [5], fatty acid oxidation [6], peroxide disproportionation [7], and oxygen reduction in cytochrome c oxidase [8]. While tyrosyl radicals, generated by photolysis in solution, decay in the microsecond time regime [9], proteins have developed ways to control radical reactivity and extend radical lifetimes. The intermediate tyrosyl radical can be detected using spectroscopic techniques, such as time-resolved optical, electron paramagnetic resonance (EPR), and vibrational spectroscopies (visible Raman, UV resonance Raman (UVRR), and reaction-induced FT-IR (RIFT-IR)). These techniques have yielded insight into the functional roles of redox-active tyrosines.

When tyrosine is oxidized, a neutral tyrosyl radical is formed [10]. It has been proposed [3] that deprotonation of the phenolic oxygen, accompanying radical formation, is important in controlling the kinetics and thermodynamics of ET under physiological conditions. Fig. 1 illustrates a reaction, in which oxidation of tyrosine is accompanied with protonation of an imidazole side group of histidine. This reaction is an example of a proton coupled electron transfer (PCET) reaction. Because proton transfer (PT) can occur only over short distances, the position, structure, and pK_a of the proton-accepting group are potentially critical factors in controlling radical transfer (for example, see

Abbreviations: Chl, chlorophyll; EPR, electron paramagnetic resonance; ET, electron transfer; NMR, nuclear magnetic resonance; OEC, oxygen evolving complex; PCET, proton coupled electron transfer; Pheo, pheophytin; PT, proton transfer; PSII, photosystem II; Q_A and Q_B, plastoquinone acceptors in PSII; RIFT-IR, reaction-induced FT-IR; RNR, ribonucleotide reductase; SIE, solvent isotope effect; UNA, unnatural amino acid; UVRR, ultraviolet resonance Raman, Y122, tyrosine 122 in the β2 subunit of RNR; YD, tyrosine 160 in the D2 polypeptide of PSII; YZ, tyrosine 161 in the D1 polypeptide of PSII; υ_{as}, asymmetric stretch, υ_s, symmetric stretch

☆ This article is part of a Special Issue entitled: Vibrational spectroscopies and bioenergetic systems.

* Tel.: +1 404 385 6085.
E-mail address: bridgette.barry@chemistry.gatech.edu.

http://dx.doi.org/10.1016/j.bbabio.2014.09.003
0005-2728/

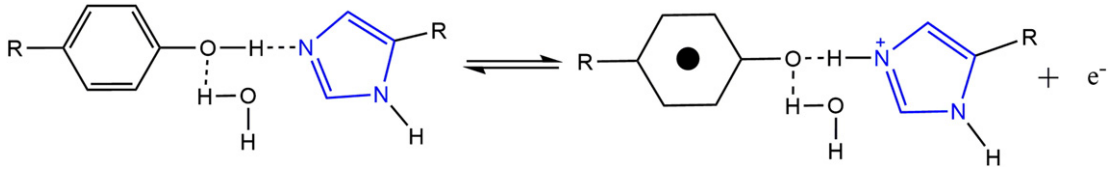

Fig. 1. Schematic diagram illustrating a PCET reaction between tyrosine and a hydrogen-bonded histidine.

discussion in [11]). The mechanisms of tyrosine-based ET and PCET reactions in DNA synthesis, photosynthesis, bioengineered proteins, and biomimetic compounds have been the subject of great interest, and some recent findings, relevant to tyrosine-based charge transfer, are reviewed here.

2. Ribonucleotide reductase

The prototypical example of a tyrosine-based charge relay occurs in ribonucleotide reductase (RNR). In all RNRs, the reduction of ribonucleotides to deoxyribonucleotides proceeds through a free radical mechanism [12]. The reaction is initiated by H atom abstraction at the ribose 3′-carbon using an active site, transient cysteine radical [13]. There are three classes of RNRs, grouped according to the redox-active cofactor that is used as the radical initiator [14,15]. Class Ia RNRs use a tyrosyl radical (Y122O•)-diferric cofactor to generate the cysteine radical. Class Ia RNRs are found in humans, viruses, and some bacteria, including *Escherichia coli*, and are composed of α2 (formerly R1) and β2 (formerly R2) subunits (reviewed in [14]).

The binding and reduction of substrate occur in the ~170 kDa α2 subunit (Fig. 2). The C439 radical generates a 3′ substrate radical by H atom abstraction from the substrate, NDP [14]. To regulate activity, class Ia α2 contains two effector sites, one termed the specificity site and the other termed the overall activity site. When bound to the activity site, dATP is a reversible inhibitor [16]. In *E. coli*, dATP binding to the activity site has been shown to form inactive, α4β4 oligomers [17–19]. Effectors, such as ATP, bind to the specificity site and promote CDP or UDP reduction [20]. Further, binding at the specificity site stimulates interactions between α2 and β2 [17–19]. Thus, RNR is a dynamic molecule that is under exquisite allosteric and oligomeric control.

In the 87 kDa *E. coli* β2 subunit, the tyrosyl radical, Y122O•, oxidizes C439 via a reversible, long distance PCET process (Fig. 2). The Y122 radical is required for activity [21] and is generated by oxygen-requiring redox reactions at a diiron cluster [22–24]. In the isolated β2 subunit, Y122O• is stable for days [25]. However, formation of an α2β2 substrate/effector complex activates Y122O• for rapid PCET (reviewed in [26]). While the chemistry of nucleotide reduction has been shown to be ~100 s^{-1} [27], the overall activity or RNR is slower and gated by structural changes (2–10 s^{-1}) [28].

Radical propagation between Y122 and C439 occurs over 35 Å between the two subunits [29,30] via a conserved pathway of aromatic side chains. The pathway involves a reversible, proton coupled electron transfer (PCET) process (β2: Y122O• ⇌ [W48] ⇌ Y356 ⇌ α2: Y731 ⇌ Y730 ⇌ C439) (reviewed in [26]). The roles of residues in the PCET pathway were elucidated using site-directed mutagenesis [31–33] and site-specific incorporation of unnatural amino acids (UNAs) [27,34–40]. Substitution of tyrosines with aminotyrosine or fluorotyrosine trapped metastable intermediates in radical transfer (reviewed in [26]).

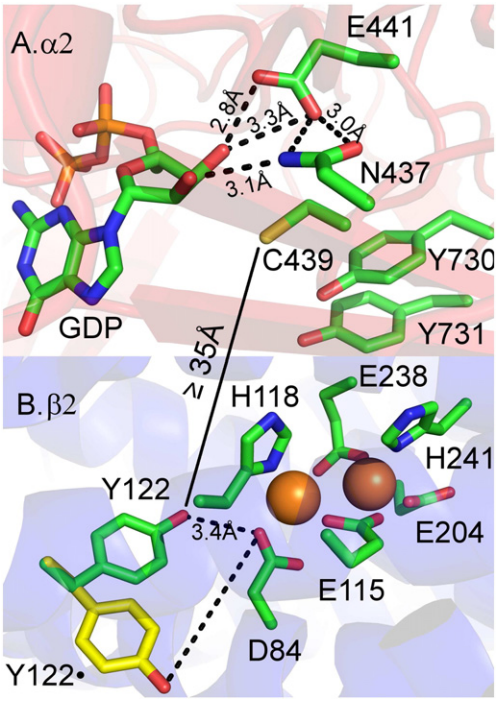

Fig. 2. Structures of the α2 and β2 subunits of RNR. (A) Active site residues in the α2 subunit at 3.2 Å (PDB 4R1R) and containing the substrate, GDP; (B) Y122OH-diferric cluster in β2 at 1.9 Å (PDB 1MXR). The solid line is the distance [29,108] between β2 Y122 and α2 C439. The proposed conformational change at Y122O• is superimposed in part B in yellow, and is described as a singlet A (backbone/ring dihedral angles: 173°/99°) to a radical B (−69°/80°) conformational change in a YT dipeptide [51]. Iron atoms are shown as orange spheres. Y356 is located in a disordered region of the β2 structure and is not shown.

3. The Y122O• radical initiator in RNR

As mentioned above, in class 1a RNR, Y122O• functions as a radical initiator in a PCET pathway that involves multiple, aromatic amino acids. The substitution of UNAs into this conserved PCET pathway (Y122 β2, Y356 β2, Y731 α2, Y730) has shown that forward ET is slightly uphill in energy and mostly likely driven by the irreversible release of water from the substrate (reviewed in [26]). At physiological pH values, tyrosine residues are expected to deprotonate when oxidized [10]. Site-specific mutagenesis has identified the pK_as of Y122, Y356, Y731, and Y730 and has shown that these residues are protonated in the pH regime in which RNR is active (pH 6–8) [41]. Therefore, PT must normally be associated with ET both in the β2 and in the α2 subunits. In the β2 subunit, experimental data suggests that PT and ET are orthogonal, meaning that the proton and electron are transferred to different acceptors. In the α2 subunit, evidence suggests that ET and PT are collinear, with the proton and electron transferring to the same acceptor (reviewed in [26,42]).

The kinetics of substrate reduction was defined in a nitrotyrosine derivative, NO_2Y122OH, in which the conformational gate is uncoupled from the chemistry of substrate reduction [27]. This NO_2Y122OH mutant conducts one enzymatic turnover, but is inactivated for multiple turnovers. However, substitution of NO_2Y at other tyrosines in the PCET pathway dramatically decreased the activity of RNR [41]. Significantly, X-ray structures of the NO_2Y α2 mutants [41] and the NO_2Y122OH mutant [27] revealed no significant structural changes relative to wildtype.

Although the midpoint potential of NO_2Y122OH is expected to be increased relative to Y122OH (~200 mV), the NO_2Y122O• species was generated by activation at the iron cluster, forming a metastable radical (~40 s half-life, 1.2 radical per β2). After mixing with substrate and effector and the α2 subunit, the NO_2Y122O• mutant generated 0.6 equivalent of dCDP and ~0.6 equivalent of a new radical on the pathway [27].

The new radical has been assigned mainly to Y356O• (85–90%), with the remainder of the radical species delocalized on Y730 and Y731 [40]. Surprisingly, this single turnover generated the phenolate form of NO_2Y122O$^-$, i.e., ET occurred without PT. Multiple turnovers are inaccessible due to thermodynamic restraints: Y356, Y731, and Y730 are unable to oxidize NO_2Y122O$^-$ in reverse PCET.

Optical titrations were used to define the pK_a of NO_2Y122OH [41]. Nitrotyrosine has unique optical bands that are sensitive to protonation of the phenolic oxygen and has a pK_a of 7.2, significantly shifted from that of tyrosine [41,43]. This study showed that the protein environment induces only small pK_a shifts (<1 pK_a unit) at most positions on the PCET pathway. However, the pK_a of NO_2Y122OH was significantly perturbed, compared to NO_2Y in aqueous solution. In fact, the pK_a of NO_2Y122OH could not be measured in a physiologically relevant pH range, but was increased by >2 pK_a units [41]. Thus, the radical initiator, Y122O•, is in an unusual environment.

The vibrational spectra of Y122O• and Y122OH have been identified [44–48]. The oxidation of tyrosine/tyrosinate to form tyrosyl radical has a distinct vibrational signature. In model tyrosyl radicals, produced by photolysis in solution or in frozen powders, a dramatic upshift of the CO vibrational band and a downshift of its aromatic ring stretching mode accompany radical formation [46,47,49]. Assignments based on UVRR spectroscopy, which resonantly enhances the bands of aromatic groups, are summarized in Table 1 [47].

RIFT-IR can also be used to monitor the oxidation of tyrosine/tyrosinate to form tyrosyl radical [45,47,48,50,51]. RIFT-IR detects tyrosyl radical and tyrosine bands, as well as other linked structural changes in the protein environments. In RIFT-IR studies, hydroxyurea [52] was used to reduce Y122O•. RIFT-IR was then employed to follow the reduction of Y122O•, constructing a difference spectrum that reflects all the structural changes induced by this reaction. These spectra reveal vibrational bands of radical and singlet states, which were assigned by $^2H_4$Y ring labeling in β2 [45]. Theoretical approaches and model compounds aided in these assignments [49,51].

When phenoxyl or tyrosyl radical is generated in aqueous solution, the CO vibrational bands are observed at 1502 and 1516 cm^{-1}, respectively (see ref [53] and Table 1). The frequency of the radical's CO band is insensitive to solvent isotope exchange with ^2H_2O [54]. However, when phenoxyl radical is formed in an argon matrix, the CO band is downshifted, compared to aqueous solution, and observed at 1481 cm^{-1} [55]. These model studies suggest that the frequency of the tyrosyl radical CO band is sensitive to hydrophobicity. The CO band of the Y122O• is detected at 1498/1499 cm^{-1} [44,45,47]. This ~17 cm^{-1} downshifted CO frequency may reflect a low, local dielectric in the environment of Y122O• (see also [41]).

For the tyrosine singlet state, the frequency of the Y7a band (Table 1) acts as a hydrogen bonding sensor, and the frequency of the Y9a band is sensitive to OH conformation [56]. The frequencies of these bands are insensitive to the solvent isotope exchange with ^2H_2O (Table 1 and [54]). Analyzing the Y122OH frequencies (p^{1}H 7.6, Table 1), Y7a is observed to be shifted, compared to aqueous tyrosinate and tyrosine, and is assigned at 1199 cm^{-1}. Y9a is also shifted, compared to aqueous tyrosinate and tyrosine, and is observed at 1170 cm^{-1} (Table 1). The unique, shifted Y7a and Y9a frequencies of Y122OH may reflect its out-of-plane OH conformation and its hydrogen bonding interaction with D84 [57]. Thus, the vibrational spectra of Y122OH and Y122O• are consistent with a hydrogen-bonded Y122OH and a non-hydrogen bonded, hydrophobic environment for Y122O•.

A remaining question concerns Y8a (aromatic ring stretching) of the radical and singlet states in RNR, which have unusual frequencies (Table 1). For example, for the tyrosine singlet (p^{1}H 8.5), the Y8a bands are observed at 1602 and 1606 cm^{-1} in ^1H_2O and ^2H_2O buffers, respectively [54]. For the Y122OH singlet in ^1H_2O at pH 7.6, the band is observed at 1608 cm^{-1} [47]. In addition, Y8a of the Y122O• radical (1556 cm^{-1}) is observed at lower frequency compared to tyrosyl radical in aqueous buffer. A substantial downshift of this band is not observed for a non-hydrogen bonded phenoxyl radical in an argon matrix. Also, the band has been reported to upshift with para substitution of the phenoxyl radical [58]. Based on calculations in ref. [49], the low frequency of the Y122O• Y8a band was tentatively attributed to a unique conformation of the radical [47]. However, recent DFT calculations at a higher level of theory on a YT dipeptide have shown that the frequencies of Y8a are relatively insensitive to conformational rearrangements in the radical and singlet states. On the other hand, Y amide bands in the YT dipeptide were shown to be exquisitely sensitive to conformation, as discussed below [51]. DFT calculations on more complex models of the Y122O•-diferric cofactor are needed to explore the unusual frequencies of these aromatic ring bands.

The species that acts as the proton donor to Y122O• in its hydrophobic environment is of interest. Theoretical studies have suggested that the proton donor for Y122O• is a water ligand to the iron cluster [59]. Evidence to support this hypothesis was obtained using an azido-labeled substrate, which functions as a suicide inhibitor of RNR [60]. In the presence of this inhibitor, Y122O• is reduced by an electron, ultimately derived from the inhibitor, and the Y122O• radical signal is quenched [61,62]. Using Mossbauer spectroscopy, evidence for a change in ligation of the iron cluster was obtained. This change in ligation was coupled to reduction of Y122O• and was assigned to a deprotonation of a water ligand. There was no evidence for an accompanying change in metal oxidation state. These studies provide experimental evidence for the involvement of water and the metal cluster in PCET reactions.

In the isolated β2 subunit, an electron hole is stored on Y122, and Y122O• is activated for facile charge transfer only in the α2β2 substrate/effector complex. The tyrosyl radical, Y122O•, is paramagnetic, and the diferric cluster is spin coupled. Thus, the tyrosyl radical gives rise to a characteristic S = 1/2 EPR spectrum [61]. Electron nuclear double resonance studies of Y122O• suggest that the radical is not hydrogen bonded [63]. Interestingly, high field EPR spectroscopy has provided evidence that Y122 is conformationally mobile. Studies of RNR single crystals predicted an oxidation-induced translation of Y122 [57]. In that study, the radical was generated by treatment of β2 crystals with hydrogen peroxide. The full rotational spectral pattern was obtained, and the orientation of the g tensor axes was determined. In that work, the EPR results showed that the g tensor was not oriented as expected from the X-ray structure of the Y122OH met state (Y122OH-diferric cluster). This finding led to the proposal that the oxidation and reduction of Y122 are associated with a translation away from D84. D84 is a unidentate ligand to the iron cluster (Fig. 2) and is hydrogen bonded to Y122OH in structures of the met state [57]. D84 is also hydrogen bonded to water ligands in the met-form of the protein. While X-ray structures of the radical state are not yet available, this predicted translation would preclude hydrogen bonding between Y122O• and D84. Such a conformational change is significant, because it rationalizes the

Table 1
Vibrational frequencies (cm^{-1}) and assignments for tyrosyl radical and singlet in RNR and model compounds, as defined by UVRR[a].

Radical			Singlet		
Sample	CO stretch Y7a	Ring stretch Y8a	CH bend Y9a	C_{ring}-CH_2-Y7a	Ring stretch Y8a
Tyr[b]	1516	1572	1174	1207	1602
Tyr[c]	N.D.[d]	N.D.	1177	1207	1602
Tyr[e]	1516	1572	1174	1207	1610
Tyr–His[b]	1516	1569	1174	1207	1602
Peptide A[b]	1516	1569	1174	1207	1602
RNR[f]	1499	1556	1170	1199	1608

[a] Reprinted with permission from *Journal of Physical Chemistry B* [47].
[b] p^{2}H 11, 244 nm probe.
[c] pH 8.5, 244 nm.
[d] N.D., not determined.
[e] p^{2}H 8.5, 244 nm [54].
[f] p^{1}H 7.6, 229 nm probe.

making and breaking of a hydrogen bond, which could modulate proton transfer from a water ligand.

RIFT-IR spectroscopy has also provided evidence that Y122 is conformationally mobile, when HU is used as a reductant for the radical. These RIFT-IR studies showed that Y122O• reduction by HU is coupled with a substantial translation of the phenolic oxygen [51]. To define the conformational change, C_1 amide labeling of tyrosine was performed, and the amide I bands of Y122O• and Y122OH were identified in the RIFT-IR spectra as bands at 1662 (Y122OH) and 1653 (Y122O•) cm^{-1}. Density functional calculations were used to predict the frequencies and ^{13}C isotope shifts, and theoretical infrared spectra were generated. Of the lowest energy conformers of radical and singlet states, the best match between experiment and theory was an A (singlet) to *B* (radical) conformational change, corresponding to a change in backbone dihedral angle (Fig. 3). The X-ray structure confirms that the Y122OH is in the A conformation. By modeling the A to *B* conformational change onto the X-ray structure of the met state, the change was concluded to be consistent with only small displacements in the amide backbone. However, the vibrational analysis and modeling suggested that the Y122 phenolic oxygen translates away from D84 in the radical state. The distance between D84 and Y122O• was predicted to be 7 Å, in qualitative agreement with previous magnetic resonance studies, which predict a 3 Å distance. These results are suggestive of a conformationally linked mechanism, which makes and breaks hydrogen bonds.

Can the predicted hydrogen bonding change at D84 be detected directly? RIFT-IR has provided evidence for such a hydrogen bonding change in D84 [50]. Again, HU was used as the reductant. The first evidence for the coupled hydrogen bonding change was obtained in the isolated β2 subunit. Isotopic labeling of aspartate with two different isotopologues was performed using an aspartate auxotrophic strain. This experiment identified the infrared bands of D84, which were concluded to be markers for hydrogen bonding changes (Table 2), and showed that structural interactions are propagated from Y122 to the metal cluster.

Table 2
D84 Vibrational Assignments in the Y122OH and the Y122O• states, as assigned by ^{13}C-Asp Labeling and RIFT-IR[a].

Y122O•			Y122OH		
υ[b]	Δυ (^{13}C)	Assignment	υ[b]	Δυ (^{13}C)	Assignment
(+) 1687	−43	D84 υ_{as}	(−) 1675	−40	D84 υ_{as}
(+) 1653	−40	D84 amide I	(−) 1661	−40	D84 amide I
(+) 1563	−12	D84 amide II	(−) 1540	−8	D84 amide II
(+) 1414	N.D.[c]	D84 υ_s	(−) 1404	N.D.[c]	D84 υ_s

[a] Reprinted with permission from the *Journal of the American Chemical Society* [50].
[b] Frequencies, in cm^{-1}, from the RIFT-IR isotope-edited spectra.
[c] Not determined.

Recently, RIFT-IR measurements were performed on the RNR quaternary complex using isotopically labeled chimeras to assign bands to α2 or to β2 [48]. The inhibitor, dATP, had a dramatic effect on these mixing-induced RIFT-IR spectra. The effects of HU on Y122 and D84 were also probed in the α2β2-containing samples. As assessed by observed vibrational bands, HU-mediated events were similar to those documented in the isolated β2 subunit [50,51]. This finding supports the conclusion that HU-mediated events at Y122 and D84 are similar in the α2β2 quaternary complex and in the isolated β2 subunit.

4. Photosystem II

Another example of tyrosine-based radical transfer occurs in the photosynthetic reaction center, photosystem II (PSII). PSII carries out the light-driven oxidation of water and reduction of plastoquinone (reviewed in [64]). PSII is a large complex enzyme (Fig. 4), which contains at least 20 protein subunits and multiple redox-active cofactors [65]. Two core subunits, which bind many of the prosthetic groups,

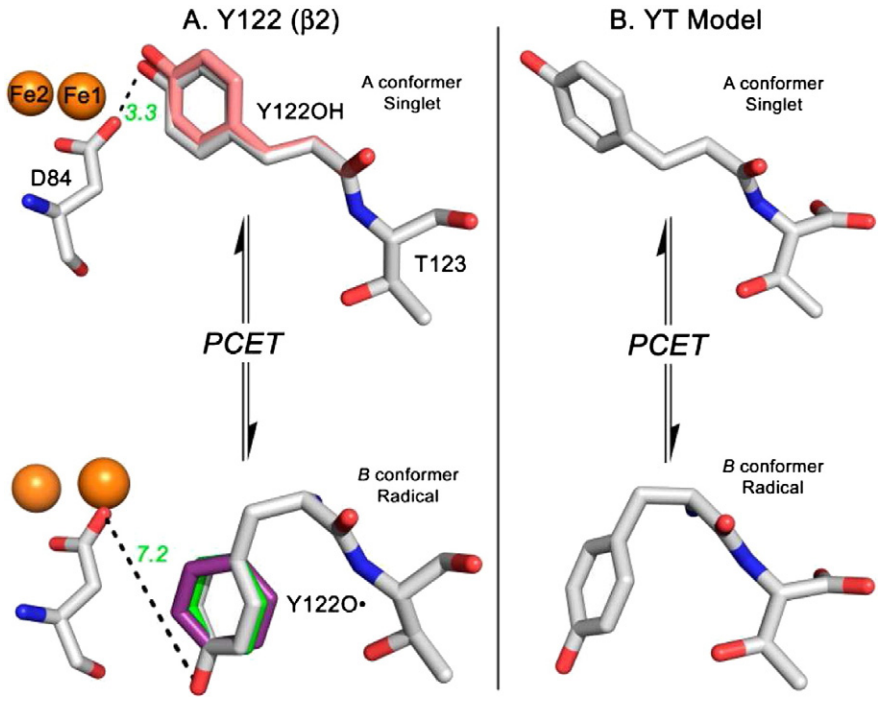

Fig. 3. Comparison of singlet and radical conformational states for Y122, as defined by HU reduction (A), and for the YT dipeptide model (B). In (A), structural refinements (see method in [51]) of the 1.4 Å met β2 (Y122OH) form (top), obtained from X-ray crystal analysis (PDB 1MXR) and of the radical (Y122O•) form (bottom). The radical form was modeled as the *B* conformer, as predicted by isotopic labeling and DFT on dipeptide models [51], and is presented in gray. Distances (in Å) between Y122 and D84 are shown in green. For the singlet (top), the dihedral angles of the A singlet conformer were also structurally refined; deviations from the met crystal structure are highlighted in pink. For Y122O• (bottom), the ring dihedral angles predicted previously from experimental [21,63] or calculated [109] hyperfine coupling constants are shown in green and purple, respectively. The structures in (B) are derived from DFT calculations on the dipeptide model.
Reprinted with permission from *Journal of Physical Chemistry B* [51].

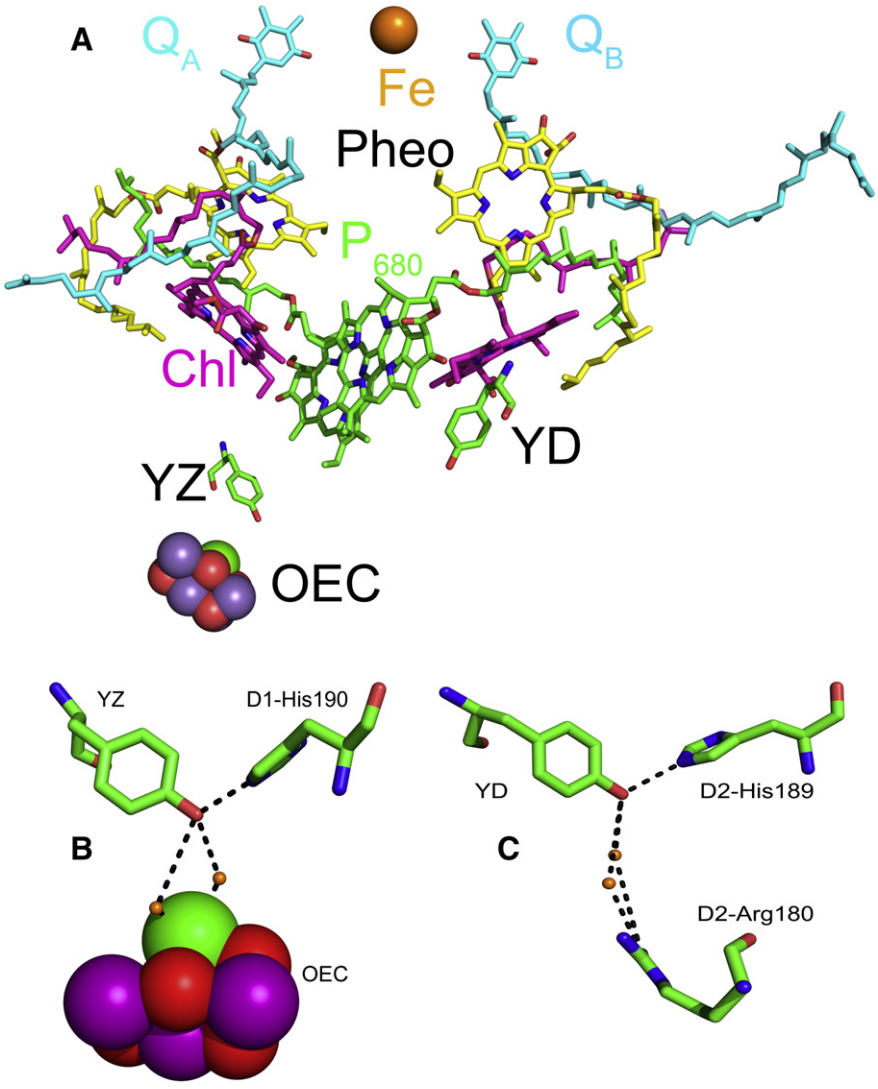

Fig. 4. (A) Cofactor arrangement in PSII from *Thermosynechococcus vulcanus* (3ARC) at 1.9 Å resolution, including YD and YZ, chlorophyll (Chl), pheophytin (Pheo), non-heme iron (Fe), and plastoquinones (Q_A and Q_B). In the oxygen evolving complex (OEC): calcium, green; manganese, purple; oxygen, red; (B) YZ and its hydrogen bonding interactions; (C) YD and its hydrogen bonding interactions. In (B and C), hydrogen bonded water molecules are depicted as orange spheres.
Reprinted with permission from *Nature Chemistry* [110].

are the D1 and D2 polypeptides. An initial photoexcitation of chlorophyll generates a charge-separated state in which a quinone acceptor (Q_A, Q_B) is reduced and a Mn_4CaO_5 cluster is oxidized. This reaction occurs across the thylakoid membrane and is mediated by a chain of redox active groups, including chlorophyll (Chl), pheophytin (Pheo), and a redox active-tyrosine YZ. YZ is tyrosine 161 of the subunit called D1 (reviewed in [66]). YZ is required for activity and mediates radical transfer between the chlorophyll donor, P_{680}^{+}, and the metal cluster, where oxygen is generated from water [67]. This metal cluster or oxygen-evolving center (OEC) accumulates four oxidizing equivalents, with YZ functioning as the relay on each flash. The sequentially oxidized states of the OEC are called the S_n states, where the subscript n refers to the number of oxidizing equivalents stored [68].

The manganese and calcium ions in the OEC are bound by six carboxylate ligands and one histidine ligand. In the recent 1.9 A structure from a thermophilic cyanobacterium, the positions of bound water molecules were predicted [65]. A network of water extending from Ca-bound and Mn-bound water molecules was assigned. Two bound waters were identified at the manganese ion denoted Mn_4, and two were identified at the calcium ion. The bound water molecules at Mn_4 and Ca are candidates to be the substrate [69,70]. These bound water molecules are connected via an extensive hydrogen-bonding network to YZ, OEC ligands, and several peptide carbonyl groups (S169, D170, G171, and F182), which are all within ~7 Å of OEC-bound water molecules. New experimental and theoretical approaches to the mechanism of water oxidation, based on the 1.9 Å structure, have been reviewed recently (see, for example, [64,71]). This article focuses on the function and structure of YZ, with special emphasis on the effect of the intact hydrogen-bonding network, as revealed in the structure [65]. Comparison of YZ to the other PSII redox-active tyrosine, YD, is of interest. YD is tyrosine 160 of the subunit called D2. Unlike YZ, YD is not essential for oxygen evolution activity. YD has a lower potential, when compared to YZ, and forms a more stable radical (reviewed in [66]). The placement of bound water molecules and proximity to the Mn_4CaO_5 cluster [65] distinguish YD and YZ (Fig. 4).

5. YD and YZ in PSII

For YD and YZ, the basis of their functional differentiation is not yet clear. For example, chemical complementation and site-directed mutagenesis have defined a role for each hydrogen-bonded histidine as a proton transfer partner [72,73]. ESEEM measurements provide evidence for a hydrogen bond between YD and histidine 189 of the D2 polypeptide [74]. But, EPR experiments on YD suggest that the pathway is

more complex. An EPR-based proton inventory was consistent with competing proton transfer pathways, one proposed to be from water and one from histidine [75]. In a proton inventory, the dependence of the rate on the mole fraction of solvent isotope is determined [76]. The results showed a multiexponential dependence that was explained by two competing pathways, at least one of which was multi-proton. Also, marked pH dependence was observed in the decay kinetics, consistent with a change in mechanism when low and high pH values were compared [77].

Interestingly, YD• has been shown to undergo a temperature-dependent, conformational relaxation [78]. The YD• radical can be generated by illumination at 10 K. Cryogenic high-field EPR measurements were used to show that when the 10 K-generated radical is warmed in the dark, a shift in the g_x component of its g tensor occurs. This component of the radical's g tensor is sensitive to electrostatic interactions. The shift in g_x tensor component was attributed to a spontaneous lengthening of the hydrogen bond to YD• [78].

Because metal removal is expected to change the environment of YZ, it is important to investigate YZ in preparations that contain the Mn_4CaO_5 cluster. YZ• has a short lifetime (microsecond to millisecond) in such preparations, because YZ• is rapidly reduced by the metal cluster [67,79]. As the essential charge relay in photosynthetic water oxidation, the midpoint potential of YZ must be carefully controlled [80]. Theoretical approaches have predicted changes in side chain pK_a, linked to the S state cycle (reviewed in [81]). Changes in pK_a and S state associated conformational dynamics [82] could play a role in facilitating electron and proton transfer through YZ.

To assess the effect of oxidation of the Mn_4CaO_5 cluster on the environment of YZ, laser flashes were used to step the OEC through its S state cycle. To extend the lifetime of YZ•, the S state of interest was generated by a flash, and then the sample was frozen to block further S transitions. For example, at 190 K, the S_2 to S_3 transition is blocked. A laser flash given to a sample prepared in the S_2 state then generates the YZ• Q_A^- state. YZ• cannot oxidize the S_2 state, but instead recombines on the seconds time scale with the quinone acceptor. The kinetics of decay was then monitored as a function of pH and solvent isotope.

In refs. [83,84], a comparison of YZ• kinetics in the S_0 and S_2 states was performed. These states correspond to a change in oxidation state of the Mn_4CaO_5 cluster S_0, $Mn(III)_3Mn(IV)_1$; S_2, $(Mn(III)_1Mn(IV)_3)$ [85]. The S_0 and S_2 states exhibited a difference in the YZ• decay rate ($t_{1/2} = 3.3 \pm 0.3$ s in S_0; $t_{1/2} = 2.1 \pm 0.3$ s in S_2) and in the solvent isotope effect (SIE) on the reaction (1.3 ± 0.3 in S_0; 2.1 ± 0.3 in S_2). The changes were attributed to oxidation-induced changes in the hydrogen-bonding network that links YZ and the Mn_4CaO_5 cluster.

Although the YZ site is known to be solvent accessible, the recombination rate and SIE were pH independent in both S states. While YD exhibited marked pH dependent kinetics, YZ• did not [75,77]. A coupled proton electron transfer, through a single transition state, can occur by such a pH independent mechanism [86,87]. In tyrosine and phenol model compounds, it has been shown that coupled proton electron transfer reactions are often thermodynamically favored, because high energy intermediates, such as the tyrosine cation radical, are avoided [88–90].

Ammonia is an inhibitor of PSII [70,91–93] and disrupts hydrogen bonding to peptide C═O groups in the OEC [94,95]. Significantly, ammonia dramatically slowed the YZ• recombination rate in the S_2 state, but had a smaller effect in the S_0 state. In contrast, ammonia had no significant effect on the decay of YD•, the more stable radical. These experiments document significant environmental effects on tyrosine-based charge relays and indicate that the hydrogen-bonding network, containing YZ, responds to the oxidation of the OEC.

6. ET and hopping in azurin, a bioengineered protein

Sensitizer-modified proteins have been used to investigate the factors that control ET rates in biological systems. In this approach, a folded protein of known structure is modified to bind a photosensitizer, which generates a strong oxidant, either in the ground (Ru) or excited (Re) state (reviewed in [96,97]). For example, to investigate the role of aromatic residues in ET, azurin, a copper-binding protein, was engineered to contain photosensitizers. In a Ru-modified azurin, Cu(I) to Ru(III) ET rates decreased exponentially with distance, consistent with a single-step tunneling mechanism (reviewed in [98]). In a Re-modified azurin, Cu(I) oxidation by the Re excited state (19 Å distance) was accelerated by two orders of magnitude when an intermediary tryptophan residue was present [99]. Tyrosine and phenylalanine substitutions did not support this hopping-induced rate increase.

Recently, the UNA, nitrotyrosine, was substituted at selected positions in Ru-modified azurin [43]. Nitrotyrosine, with its pK_a of 7.2, undergoes ET, not PCET, at physiologically pH values. Three nitrotyrosine derivatives were studied. Rates increased by a factor of 10–50 compared to singlet step ET without the nitrotyrosine. The observed rate enhancements for the three nitrotyrosine variants were in good agreement with hopping maps, generated based on semiclassical ET theory and parameters (reorganization energies, electronic couplings, and distance dependence) from similar systems [43].

7. Biomimetics and redox active tyrosines

To model the interactions of tyrosine charge relays with the protein matrix, biomimetic compounds offer advantages. The model systems are structurally well defined. This approach has been used to model iron sulfur proteins and heme-binding proteins, as well as redox-active tyrosines (for examples, see [100–102]). Recent biomimetic studies pertinent to the YD, YZ, and Y122 radicals are summarized below.

In the recent work [103], a structured, three alpha helical bundle, called α3, was used to test the effect of a hydrophobic environment on the midpoint potential of the UNA, 3,5-fluorotyrosine (3,5-F_2Y). Tyrosyl radicals generated in the α3 *de novo*-designed peptide are relatively stable, and the environment of the radical was shown to be hydrophobic [104]. The UNA exhibited reversible electrochemical behavior in this environment, which was designed to mimic the secondary structural environment of Y122 in the β2 subunit. Importantly, α3-Y or α3-3,5F_2Y exhibited increased midpoint potentials at pH 7.0 (150–180 mV), relative to model compounds in aqueous solution. Thus, a hydrophobic protein environment was shown to have a substantial effect on the reduction potential. In the α3 peptide, Y and 3,5 F_2Y were shown to have midpoint potentials that differed by 30 mV.

In ref. [105] a hybrid system, containing benzimidazole–phenol porphyrin moeties, was attached to TiO_2. The benzimidazole–phenol species is designed as a mimic of a tyrosine–histidine pair, as found in PSII. Irradiation of this compound led to a charge separation between the porphyrin and TiO_2. A second ET reaction from the benzimidazole–phenol group to the oxidized porphyrin then occurred. This second ET was accompanied by PT from the phenol to benzimidazole group. High-field EPR measurements were used to show that the resulting phenoxyl radical is neutral, but hydrogen bonded. Annealing the sample resulted in a shift of the g_x component of the phenoxyl radical. This annealing effect is similar to the conformational relaxation, previously reported for the YD radical in PSII [78]. Based on electronic structure calculations, this change was interpreted as a spontaneous alteration in hydrogen bond strength, which is caused by a temperature-dependent solvation change.

In refs. [106,107], a *de novo*-designed peptide was synthesized to mimic PCET between tyrosine and histidine (Fig. 5). This 18 amino acid beta hairpin maquette (peptide A), contains a single histidine and tyrosine. The NMR structure showed that histidine and tyrosine interact via a pi–pi interaction. A tyrosyl radical was formed by UV photolysis or electrochemically. Square wave voltammetry as a function of pH provided evidence for a proton transfer from tyrosine to histidine. These inflection points were absent in a variant in which cyclohexylalanine was substituted for histidine. This beta hairpin scaffold is robust to substitutions, and mutations were generated at other charged residues,

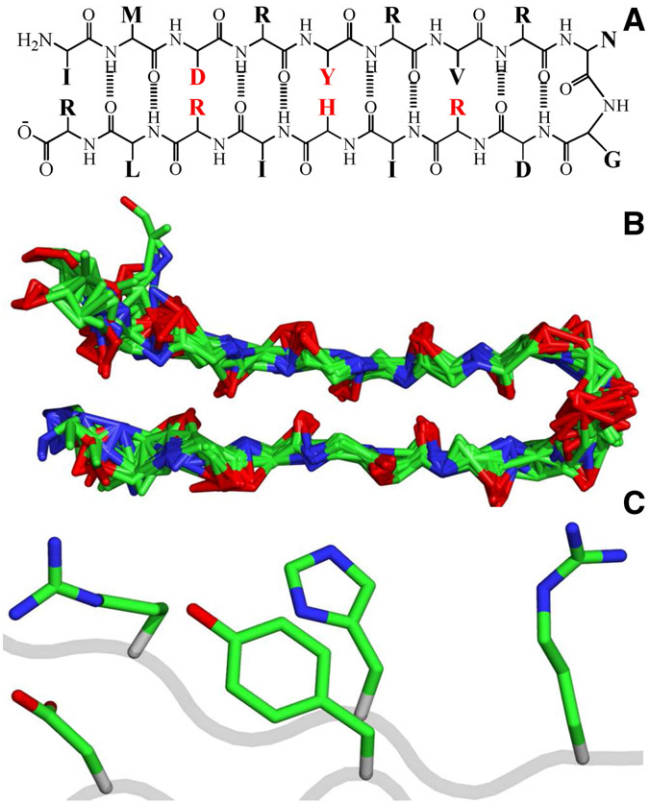

Fig. 5. (A) Primary sequence of peptide A, IMDRYRVRNGDRIHIRLR. The residues involved in the cross-strand interaction are in red; (B) Lowest-energy NMR structures of peptide A [106]; (C) Intermolecular interactions in the lowest-energy structure of peptide A showing cross-strand interactions between Y5 and H14 (π–π), Y5 and R12 (π–cation), Y5 and R16 (H-bond), and the salt-bridge formed by D3 and R16. See [54] for more details.

showing that a pi–cation interaction with arginine decreased the peak potential of the tyrosine. This change mimics the lower potential of YD, which is distinguished from YZ by pi–cation interactions with arginine residues [65]. Interestingly, UV resonance Raman spectroscopy detected a redox-induced secondary structural change in the peptide [54]. This conformational change was reversible. Thus, in the case of this beta hairpin maquette, the protein environment is dynamic and responds to charge transfer.

8. Summary

These results document the exquisite control of PCET in native systems, involving redox-coupled changes in distance, secondary structure, and hydrogen bonding. In RNR, there is evidence for redox-coupled mobility in the radical initiator, at least under two sets of conditions, reduction with HU and generation of the radical with H_2O_2. In PSII, the YZ and YD PCET mechanisms are distinct in their pH dependence, suggesting a significant effect of the protein environment on the thermodynamics and kinetics of PCET. YD exhibits a spontaneous, temperature-dependent relaxation, which may correspond to lengthening of a hydrogen bond. In addition, the kinetics of YZ decay are responsive to photooxidation reactions at the metal center. This literature also illustrates the power of biomimetics, which can be used to obtain more insight into events on the PCET pathway. Bioengineered proteins and peptides have provided new information about hopping mechanism and charge transfer.

Acknowledgments

This study was financially supported by NSF CHE-1213350 and NSF MCB-1411734. The author thanks Mr. Zhanjun Guo, Dr. Adam Offenbacher, and Dr. Cynthia Pagba for assistance with figures. B.A.B. thanks her past and present students, postdocs, and coworkers. She is also grateful to Prof. J. Stubbe and Prof. D. Sherrill and their research groups for helpful discussions.

References

[1] J.L. Dempsey, J.R. Winkler, H.B. Gray, Proton-coupled electron flow in protein redox machines, Chem. Rev. 110 (2010) 7024–7039.
[2] C.C. Moser, J.M. Keske, K. Warncke, R.S. Farid, P.L. Dutton, Nature of biological electron transfer, Nature 355 (1992) 796–802.
[3] S.Y. Reece, J.M. Hodgkiss, J. Stubbe, D.G. Nocera, Proton-coupled electron transfer: the mechanistic underpinning for radical transport and catalysis in biology, Phil. Trans. R. Soc. B 361 (2006) 1351–1364.
[4] M.M. Whittaker, J.W. Whittaker, Tyrosine-derived free radical in apogalactose oxidase, J. Biol. Chem. 265 (1990) 9610–9613.
[5] J.M. Lu, C.E. Rogge, G. Wu, R.J. Kulmacz, W.A. van der Donk, A.L. Tsai, Cyclooxygenase reaction mechanism of PGHS—evidence for a reversible transition between a pentadienyl radical and a new tyrosyl radical by nitric oxide trapping, J. Inorg. Biochem. 105 (2011) 356–365.
[6] A. Gupta, A. Mukherjee, K. Matsui, J.P. Roth, Evidence for protein radical-mediated nuclear tunneling in fatty acid alpha-oxygenase, J. Am. Chem. Soc. 130 (2008) 11274–11275.
[7] X. Zhao, J. Suarez, A. Khajo, S. Yu, L. Metlitsky, R.S. Magliozzo, A radical on the Met-Tyr-Trp modification required for catalase activity in catalase-peroxidase is established by isotopic labeling and site-directed mutagenesis, J. Am. Chem. Soc. 132 (2010) 8268–8269.
[8] P. Hellwig, U. Pfitzner, J. Behr, B. Rost, R.P. Pesavento, W.A. van der Donk, R.B. Gennis, H. Michel, B. Ludwig, W. Mäntele, Vibrational modes of tyrosine in cytochrome c oxidase from *Paracoccus denitrificans*: FTIR and electrochemical studies on Tyr-D_4-labeled and on Tyr280His and Tyr35Phe mutant enzymes, Biochemistry 41 (2002) 9116–9125.
[9] J.A. Cappuccio, I. Ayala, G.I. Elliot, I. Szundi, J. Lewis, J.P. Konopelski, B.A. Barry, Ó. Einarsdóttir, Modeling the active site of cytochrome oxidase: synthesis and characterization of a cross-linked histidine-phenol, J. Am. Chem. Soc. 124 (2002) 1750–1760.
[10] W.T. Dixon, D. Murphy, Determination of the acidity constants of some phenol radical cations by means of electron spin resonance, J. Chem. Soc. Lond. Faraday Trans. II 72 (1976) 1221–1230.
[11] S. Hammes-Schiffer, A.V. Soudackov, Proton-coupled electron transfer in solution, proteins, and electrochemistry, J. Phys. Chem. B 112 (2008) 14108–14123.
[12] J. Stubbe, W.A. van der Donk, Ribonucleotide reductases: radical enzymes with suicidal tendencies, Chem. Biol. 2 (1995) 793–801.
[13] J. Stubbe, Ribonucleotide reductases: amazing and confusing, J. Biol. Chem. 265 (1990) 5329–5332.
[14] A. Jordan, P. Reichard, Ribonucleotide reductases, Ann. Rev. Biochem. 67 (1998) 71–98.
[15] J.A. Cotruvo, J. Stubbe, Class I ribonucleotide reductases: metallocofactor assembly and repair in vitro and in vivo, Ann. Rev. Biochem. 80 (2011) 733–767.
[16] A. Larsson, P. Reichard, Enzyme synthesis of deoxyribonucleotides IX. Allosteric effects in the reduction of pyrimidine ribonucleotides by the ribonucleoside diphosphate reductase system of *Escherichia coli*, J. Biol. Chem. 241 (1966) 2533–2539.
[17] R. Rofougaran, M. Crona, M. Vodnala, B.M. Sjoberg, A. Hofer, Oligomerization status directs overall activity regulation of the *Escherichia coli* class Ia ribonucleotide reductase, J. Biol. Chem. 283 (2008) 35310–35318.
[18] N. Ando, E.J. Brignole, C.M. Zimanyi, M.A. Funk, K. Yokoyama, F.J. Asturias, J. Stubbe, C.L. Drennan, Structural interconversions modulate activity of *Escherichia coli* ribonucleotide reductase, Proc. Nat. Acad. Sci. U. S. A. 108 (2011) 21046–21051.
[19] C.M. Zimanyi, N. Ando, E.J. Brignole, F.J. Asturias, J. Stubbe, C.L. Drennan, Tangled up in knots: structures of inactivated forms of *E. coli* class Ia ribonucleotide reductase, Structure 20 (2012) 1374–1383.
[20] P. Reichard, Ribonucleotide reductases: substrate specificity by allostery, Biochem. Biophys. Res. Commun. 396 (2010) 19–23.
[21] B.-M. Sjoberg, P. Reichard, A. Graslund, A. Ehrenberg, The tyrosine free radical in ribonucleotide reductase from *Escherichia Coli*, J. Biol. Chem. 253 (1978) 6863–6865.
[22] C.L. Atkin, L. Thelander, P. Reichard, G. Lang, Iron and free radical in ribonucleotide reductase: exchange of iron and Mössbauer spectroscopy of the protein B2 subunit of the *Escherichia coli* enzyme, J. Biol. Chem. 248 (1973) 7464–7472.
[23] A. Larsson, B.M. Sjöberg, Identification of the stable free radical tyrosine residue in ribonucleotide reductase, EMBO J. 5 (1986) 2037–2040.
[24] J.M. Bollinger Jr., D.E. Edmondson, B.H. Huynh, J. Filley, J.R. Norton, J. Stubbe, Mechanism of assembly of the tyrosyl radical-dinuclear iron cluster cofactor of ribonucleotide reductase, Science 253 (1991) 292–298.
[25] A. Graslund, A. Ehrenberg, L. Thelander, Characterization of the free radical of mammalian ribonucleotide reductase, J. Biol. Chem. 257 (1982) 5711–5715.
[26] E.C. Minnihan, D.G. Nocera, J. Stubbe, Reversible, long-range radical transfer in *E. coli* class Ia ribonucleotide reductase, Acc. Chem. Res. 46 (2013) 2524–2535.
[27] K. Yokoyama, U. Uhlin, J. Stubbe, A hot oxidant, 3-NO2Y122 radical, unmasks conformational gating in ribonucleotide reductase, J. Am. Chem. Soc. 132 (2010) 15368–15379.
[28] J. Ge, G. Yu, M.A. Ator, J. Stubbe, Pre-steady-state and steady-state kinetic analysis of *E. coli* class I ribonucleotide reductase, Biochemistry 42 (2003) 10071–10083.
[29] M. Bennati, J.H. Robblee, V. Mugnaini, J. Stubbe, J.H. Freed, P. Borbat, EPR distance measurements support a model for long-range radical initiation in *E. coli* ribonucleotide reductase, J. Am. Chem. Soc. 127 (2005) 15014–15015.

[30] M.R. Seyedsayamdost, C.T.Y. Chan, V. Mugnaini, J. Stubbe, M. Bennati, PELDOR spectroscopy with DOPA, J. Am. Chem. Soc. 129 (2007) 15748–15749.
[31] U. Rova, K. Goodtzova, R. Ingemarson, G. Behravan, A. Graslund, L. Thelander, Evidence by site-directed mutagenesis supports long-range electron transfer in mouse ribonucleotide reductase, Biochemistry 34 (1995) 4267–4275.
[32] M. Ekberg, M. Sahlin, M. Eriksson, B.-M. Sjöberg, Two conserved tyrosine residues in protein R1 participate in an intermolecular electron transfer in ribonucleotide reductase, J. Biol. Chem. 271 (1996) 20655–20659.
[33] U. Rova, A. Adrait, S. Pötsch, A. Gräslund, L. Thelander, Evidence by mutagenesis that Tyr370 of the mouse ribonucleotide reductase R2 protein is the connecting link in the intersubunit radical transfer pathway, J. Biol. Chem. 274 (1999) 23746–23751.
[34] C.S. Yee, M.C. Chang, J. Ge, D.G. Nocera, J. Stubbe, 2,3-difluorotyrosine at position 356 of ribonucleotide reductase R2: a probe of long-range proton-coupled electron transfer, J. Am. Chem. Soc. 125 (2003) 10506–10507.
[35] M.R. Seyedsayamdost, C.S. Yee, S.Y. Reece, D.G. Nocera, J. Stubbe, pH rate profiles of FnY356-R2s (n = 2, 3, 4) in *Escherichia coli* ribonucleotide reductase: evidence that Y-356 is a redox-active amino acid along the radical propagation pathway, J. Am. Chem. Soc. 128 (2006) 1562–1568.
[36] M.R. Seyedsayamdost, J. Stubbe, Site-specific replacement of Y-356 with 3,4-dihydroxyphenylalanine in the beta2 subunit of *E. coli* ribonucleotide reductase, J. Am. Chem. Soc. 128 (2006) 2522–2523.
[37] M.R. Seyedsayamdost, J. Xie, C.T.Y. Chan, P.G. Schultz, J. Stubbe, Site-specific insertion of 3-aminotyrosine into subunit alpha 2 of *E-coli* ribonucleotide reductase: direct evidence for involvement of Y-730 and Y-731 in radical propagation, J. Am. Chem. Soc. 129 (2007) 15060–15071.
[38] E.C. Minnihan, M.R. Seyedsayamdost, U. Uhlin, J. Stubbe, Kinetics of radical intermediate formation and deoxynucleotide production in 3-aminotyrosine-substituted *Escherichia coli* ribonucleotide reductases, J. Am. Chem. Soc. 133 (2011) 9430–9440.
[39] E.C. Minnihan, D.D. Young, P.G. Schultz, J. Stubbe, Incorporation of fluorotyrosines into ribonucleotide reductase using an evolved, polyspecific aminoacyl-tRNA synthetase, J. Am. Chem. Soc. 133 (2011) 15942–15945.
[40] K. Yokoyama, A.A. Smith, B. Corzilius, R.G. Griffin, J. Stubbe, Equilibration of tyrosyl radicals (Y356*, Y731*, Y730*) in the radical propagation pathway of the *Escherichia coli* class Ia ribonucleotide reductase, J. Am. Chem. Soc. 133 (2011) 18420–18432.
[41] K. Yokoyama, U. Uhlin, J. Stubbe, Site-specific incorporation of 3-nitrotyrosine as a probe of pK_a perturbation of redox-active tyrosines in ribonucleotide reductase, J. Am. Chem. Soc. 132 (2010) 8385–8397.
[42] J. Stubbe, D.G. Nocera, C.S. Yee, M.C.Y. Chang, Radical initiation in the class I ribonucleotide reductase: long-range proton-coupled electron transfer? Chem. Rev. 103 (2003) 2167–2201.
[43] J.J. Warren, N. Herrera, M.G. Hill, J.R. Winkler, H.B. Gray, Electron flow through nitrotyrosinate in *Pseudomonas aeruginosa* azurin, J. Am. Chem. Soc. 135 (2013) 11151–11158.
[44] G. Backes, M. Sahlin, B.-M. Sjoberg, T.M. Loehr, J. Sanders-Loehr, Resonance Raman spectroscopy of ribonucleotide reductase. Evidence for a deprotonated tyrosyl radical and photochemistry of the binuclear iron center, Biochemistry 28 (1989) 1923–1929.
[45] A.R. Offenbacher, I.R. Vassiliev, M.R. Seyedsayamdost, J. Stubbe, B.A. Barry, Redox-linked structural changes in ribonucleotide reductase, J. Am. Chem. Soc. 131 (2009) 7496–7497.
[46] A.R. Offenbacher, J. Chen, B.A. Barry, Perturbations of aromatic amino acids are associated with iron cluster assembly in ribonucleotide reductase, J. Am. Chem. Soc. 133 (2011) 6978–6988.
[47] B.A. Barry, J. Chen, J. Keough, D. Jenson, A. Offenbacher, C. Pagba, Proton coupled electron transfer and redox active tyrosines: structure and function of the tyrosyl radicals in ribonucleotide reductase and photosystem II, J. Phys. Chem. Lett. 3 (2012) 543–554.
[48] A.R. Offenbacher, R.A. Watson, C.V. Pagba, B.A. Barry, Redox-dependent structural coupling between the α2 and β2 Subunits in *E. coli* ribonucleotide reductase, J. Phys. Chem. B 118 (2014) 2993–3004.
[49] K. Range, I. Ayala, D. York, B.A. Barry, Normal modes of redox-active tyrosine: conformation dependence and comparison to experiment, J. Phys. Chem. B 110 (2006) 10970–10981.
[50] A.R. Offenbacher, E.C. Minnihan, J. Stubbe, B.A. Barry, Redox-linked changes to the hydrogen-bonding network of ribonucleotide reductase beta2, J. Am. Chem. Soc. 135 (2013) 6380–6383.
[51] A.R. Offenbacher, L.A. Burns, C.D. Sherrill, B.A. Barry, Redox-linked conformational control of proton-coupled electron transfer: Y122 in the ribonucleotide reductase beta2 subunit, J. Phys. Chem. B 117 (2013) 8457–8468.
[52] J. Shao, X. Liu, L. Zhu, Y. Yen, Targeting ribonucleotide reductase for cancer therapy, Expert Opin. Ther. Targets 17 (2013) 1423–1437.
[53] C.R. Johnson, M. Ludwig, S.A. Asher, Ultraviolet resonance Raman characterization of photochemical transients of phenol, tyrosine, and tryptophan, J. Am. Chem. Soc. 108 (1986) 905–912.
[54] C.V. Pagba, B.A. Barry, Redox-induced conformational switching in photosystem-II-inspired biomimetic peptides: a UV resonance Raman study, J. Phys. Chem. B 116 (2012) 10590–10599.
[55] J. Spanget-Larsen, M. Gil, A. Gorski, D.M. Blake, J. Waluk, J.G. Radziszewski, Vibrations of the phenoxyl radical, J. Am. Chem. Soc. 123 (2001) 11253–11261.
[56] H. Takeuchi, N. Watanabe, Y. Satoh, I. Harada, Effects of hydrogen bonding on the tyrosine Raman bands in the 1300–1150 cm^{-1} region, J. Raman Spectrosc. 20 (1989) 233–237.
[57] M. Högbom, M. Galander, M. Andersson, M. Kolberg, W. Hofbauer, G. Lassmann, P. Nordlund, F. Lendzlan, Displacement of the tyrosyl radical cofactor in ribonucleotide reductase obtained by single-crystal high-field EPR and 1.4-A X-ray data, Proc. Natl. Acad. Sci. 100 (2003) 3209–3214.
[58] R. Schnepf, A. Sokolowski, J. Miller, V. Bachler, K. Wieghardt, P. Hildebrandt, Resonance Raman spectroscopic study of phenoxyl radical complexes, J. Am. Chem. Soc. 120 (1998) 2352–2364.
[59] W.G. Han, L. Noodleman, DFT calculations for intermediate and active states of the diiron center with a tryptophan or tyrosine radical in *Escherichia coli* ribonucleotide reductase, Inorg. Chem. 50 (2011) 2302–2320.
[60] B. Wörsdörfer, D.A. Conner, K. Yokoyama, J. Livada, M.R. Seyedsayamdost, W. Jiang, A. Silakov, J. Stubbe, J.M. Bollinger Jr., C. Krebs, Function of the diiron cluster of *Escherichia coli* class Ia ribonucleotide reductase in proton-coupled electron transfer, J. Am. Chem. Soc. 135 (2013) 8585–8593.
[61] B.M. Sjoberg, A. Graslund, F. Eckstein, A substrate radical intermediate in the reaction between ribonucleotide reductase from *Escherichia coli* and 2′-azido-2′-deoxynucleoside diphosphates, J. Biol. Chem. 258 (1983) 8060–8067.
[62] W.A. van der Donk, G. Yu, D.J. Silva, J. Stubbe, J.R. McCarthy, E.T. Jarvi, D.P. Matthews, R.J. Resvick, E. Wagner, Inactivation of ribonucleotide reductase by (E)-2′-fluoromethylene-2′-deoxycytidine 5′-diphosphate: a paradigm for nucleotide mechanism-based inhibitors, Biochemistry 35 (1996) 8381–8391.
[63] C.J. Bender, M. Sahlin, G.T. Babcock, B.A. Barry, T.K. Chandrashekar, S.P. Salowe, J.A. Stubbe, B. Lindstrom, L. Petersson, A. Ehrenberg, B.-M. Sjoberg, An ENDOR study of the tyrosyl free radical in ribonucleotide reductase from *Escherichia coli*, J. Am. Chem. Soc. 111 (1989) 8076–8083.
[64] N. Cox, D.A. Pantazis, F. Neese, W. Lubitz, Biological water oxidation, Acc. Chem. Res. 46 (2013) 1588–1596.
[65] Y. Umena, K. Kawakami, J.-R. Shen, N. Kamiya, Crystal structure of oxygen-evolving photosystem II at a resolution of 1.9 Angstrom, Nature 473 (2011) 55–60.
[66] B.A. Barry, Proton coupled electron transfer and redox active tyrosines in photosystem II, J. Photochem. Photobiol. B 104 (2011) 60–71.
[67] S. Gerken, K. Brettel, E. Schlodder, H.T. Witt, Optical characterization of the immediate donor to Chlorophyll a_{II}^{+} in O_2-evolving photosystem II complexes, FEBS Lett. 237 (1988) 69–75.
[68] P. Joliot, B. Kok, Oxygen evolution in photosynthesis, in: Govindjee (Ed.), Bioenergetics of PhotosynthesisAcademic Press, New York, 1975, pp. 388–412.
[69] K. Kawakami, Y. Umena, N. Kamiya, J.R. Shen, Structure of the catalytic, inorganic core of oxygen-evolving photosystem II at 1.9 angstrom resolution, J. Photochem. Photobiol. B (2011) 9–18.
[70] M. Perez Navarro, W.M. Ames, H. Nilsson, T. Lohmiller, D.A. Pantazis, L. Rapatskiy, M.M. Nowaczyk, F. Neese, A. Boussac, J. Messinger, W. Lubitz, N. Cox, Ammonia binding to the oxygen-evolving complex of photosystem II identifies the solvent-exchangeable oxygen bridge (mu-oxo) of the manganese tetramer, Proc. Natl. Acad. Sci. U. S. A. 110 (2013) 15561–15566.
[71] H. Dau, I. Zaharieva, M. Haumann, Recent developments in research on water oxidation by photosystem II, Curr. Opin. Chem. Biol. 16 (2012) 3–10.
[72] S. Kim, J. Liang, B.A. Barry, Chemical complementation identifies a proton acceptor for redox-active tyrosine D in photosystem II, Proc. Natl. Acad. Sci. U. S. A. 94 (1997) 14406–14411.
[73] A.-M.A. Hays, I.R. Vassiliev, J.H. Golbeck, R.J. Debus, Role of D1-His190 in proton-coupled electron transfer reactions in photosystem II: a chemical complementation study, Biochemistry 37 (1998) 11352–11365.
[74] K.A. Campbell, J.M. Peloquin, B.A. Diner, X.-S. Tang, D.A. Chisholm, R.D. Britt, The τ-nitrogen of D2 histidine 189 is the hydrogen bond donor to the tyrosine radical YD of photosystem II, J. Am. Chem. Soc. 119 (1997) 4787–4788.
[75] D. Jenson, B.A. Barry, Proton-coupled electron transfer in photosystem II: proton inventory of a redox active tyrosine, J. Am. Chem. Soc. 131 (2009) 10567–10573.
[76] K.S. Venkatasubban, R.L. Schowen, The proton inventory technique, in: G.D. Fasman (Ed.), Critical Reviews in Biochemistry, CRC Press, Boca Raton, 2000, pp. 1–44.
[77] D. Jenson, A. Evans, B.A. Barry, Proton-coupled electron transfer and tyrosine D of photosystem II, J. Phys. Chem. B 111 (2007) 12599–12604.
[78] P. Faller, C. Goussias, A.W. Rutherford, S. Un, Resolving intermediates in biological proton-coupled electron transfer: a tyrosyl radical prior to proton movement, Proc. Natl. Acad. Sci. U. S. A. 100 (2003) 8732–8735.
[79] R.E. Blankenship, G.T. Babcock, J.T. Warden, K. Sauer, Observation of a new EPR transient in chloroplasts that may reflect the electron donor to photosystem II at room temperature, FEBS Lett. 51 (1975) 287–293.
[80] N. Ioannidis, G. Zahariou, V. Petrouleas, The EPR spectrum of tyrosine Z• and its decay kinetics in O_2-evolving photosystem II preparations, Biochemistry 47 (2008) 6292–6300.
[81] F.M. Ho, Structural and mechanistic investigations of photosystem II through computational methods, Biochim. Biophys. Acta 1817 (2012) 106–120.
[82] M. Miqyass, H.J. van Gorkom, C.F. Yocum, The PSII calcium site revisited, Photosynth. Res. 92 (2007) 275–287.
[83] J. Keough, D.L. Jenson, A. Zuniga, B.A. Barry, Proton coupled electron transfer and redox-active tyrosine Z in the photosynthetic oxygen evolving complex, J. Am. Chem. Soc. 133 (2011) 11084–11087.
[84] J. Keough, A. Zuniga, D.L. Jenson, B.A. Barry, Redox control and hydrogen bonding networks: proton-coupled electron transfer reactions and tyrosine Z in the photosynthetic oxygen-evolving complex, J. Phys. Chem. B 117 (2013) 1296–1307.
[85] A. Grundmeier, H. Dau, Structural models of the manganese complex of photosystem II and mechanistic implications, Biochim. Biophys. Acta 1817 (2012) 88–105.
[86] J. Bonin, C. Costentin, C. Louault, M. Robert, M. Routier, J.-M. Savéant, Intrinsic reactivity and driving force dependence in concerted proton-electron transfers to water illustrated by phenol oxidation, Proc. Natl. Acad. Sci. U. S. A. 107 (2010) 3367–3372.
[87] M. Sjödin, T. Irebo, J.E. Utas, J. Lind, G. Merényi, B. Akermark, L. Hammarström, Kinetic effects of hydrogen bonds on proton-coupled electron transfer from phenols, J. Am. Chem. Soc. 128 (2006) 13076–13083.

[88] I.J. Rhile, T.F. Markle, H. Nagao, A.G. DiPasquale, O.P. Lam, M.A. Lockwood, K. Rotter, J.M. Mayer, Concerted proton–electron transfer in the oxidation of hydrogen bonded phenols, J. Am. Chem. Soc. 128 (2006) 6075–6088.
[89] T. Irebo, S.Y. Reece, M. Sjödin, D.G. Nocera, L. Hammarström, Proton-coupled electron transfer of tyrosine oxidation: buffer dependence and parallel mechanisms, J. Am. Chem. Soc. 129 (2007) 15462–15464.
[90] J. Bonin, C. Costentin, M. Robert, J.M. Saveant, C. Tard, Hydrogen-bond relays in concerted proton–electron transfers, Acc. Chem. Res. 45 (2011) 372–381.
[91] P.O. Sandusky, C.F. Yocum, The mechanism of amine inhibition of the photosynthetic oxygen evolving complex, FEBS Lett. 162 (1983) 339–343.
[92] R.D. Britt, J.-L. Zimmermann, K. Sauer, M.P. Klein, Ammonia binds to the catalytic Mn of the oxygen-evolving complex of photosystem II: evidence by electron spin-echo envelope modulation spectroscopy, J. Am. Chem. Soc. 111 (1989) 3522–3532.
[93] A. Boussac, A.W. Rutherford, S. Styring, Interaction of ammonia with the water splitting enzyme of photosystem II, Biochemistry 29 (1990) 24–32.
[94] B.C. Polander, B.A. Barry, A hydrogen-bonding network plays a catalytic role in photosynthetic oxygen evolution, Proc. Natl. Acad. Sci. U. S. A. 109 (2012) 6112–6117.
[95] B.C. Polander, B.A. Barry, Detection of an intermediary, protonated water cluster in photosynthetic oxygen evolution, Proc. Natl. Acad. Sci. U. S. A. 110 (2013) 10634–10639.
[96] J.R. Winkler, H.B. Gray, Electron flow through metalloproteins, Chem. Rev. 114 (2014) 3369–3380.
[97] J.R. Winkler, H.B. Gray, Long-range electron tunneling, J. Am. Chem. Soc. 136 (2014) 2930–2939.
[98] H.B. Gray, J.R. Winkler, Electron tunneling through proteins, Q. Rev. Biophys. 36 (2003) 341–372.
[99] C. Shih, A.K. Museth, M. Abrahamsson, A.M. Blanco-Rodriguez, A.J. Di Bilio, J. Sudhamsu, B.R. Crane, K.L. Ronayne, M. Towrie, A. Vlcek Jr., J.H. Richards, J.R. Winkler, H.B. Gray, Tryptophan-accelerated electron flow through proteins, Science 320 (2008) 1760–1762.
[100] C. Tommos, J. Skalicky, D.L. Pilloud, A.J. Wand, L.P. Dutton, De novo proteins as models of radical enzymes, Biochemistry 38 (1999) 9495–9507.
[101] M.L. Kennedy, B.R. Gibney, Proton coupling to $[4Fe\text{-}4S]^{2+/+}$ and $[4Fe\text{-}4Se]^{2+/+}$ oxidation and reduction in a designed protein, J. Am. Chem. Soc. 124 (2002) 6826–6827.
[102] C.J. Reedy, B.R. Gibney, Heme protein assemblies, Chem. Rev. 104 (2004) 617–650.
[103] K.R. Ravichandran, L. Liang, J. Stubbe, C. Tommos, Formal reduction potential of 3,5-difluorotyrosine in a structured protein: insight into multistep radical transfer, Biochemistry 52 (2013) 8907–8915.
[104] M.C. Martinez-Rivera, W. Berry Bruce, K.G. Valentine, K. Westerlund, S. Hay, C. Tommos, Electrochemical and structural properties of a protein system designed to generate tyrosine Pourbaix diagrams J, Am. Chem. Soc. 133 (2011) 17786–17795.
[105] J.D. MegiattoJr, D.D. Méndez-Hernández, M.E. Tejeda-Ferrari, A.-L. Teillout, M.J. Llansola-Portolés, G. Kodis, O.G. Poluektov, T. Rajh, V. Mujica, T.L. Groy, D. Gust, T.A. Moore, A.L. Moore, A bioinspired redox relay that mimics radical interactions of the Tyr–His pairs of photosystem II, Nat. Chem. 6 (2014) 423–428.
[106] R.S. Sibert, M. Josowicz, F. Porcelli, G. Veglia, K. Range, B.A. Barry, Proton-coupled electron transfer in biomimetic peptide as a model of enzyme regulatory mechanism, J. Am. Chem. Soc. 129 (2007) 4393–4400.
[107] R.S. Sibert, M. Josowicz, B.A. Barry, Control of proton and electron transfer in de novo designed, biomimetic β hairpins, ACS Chem. Biol. 5 (2010) 1157–1168.
[108] U. Uhlin, H. Eklund, Structure of ribonucleotide reductase protein R1, Nature 370 (1994) 533–539.
[109] F. Himo, A. Graslund, L.A. Eriksson, Density functional calculations on model tyrosyl radicals, Biophys. J. 72 (1997) 1556–1567.
[110] B.A. Barry, Proton-coupled electron transfer: free radicals under control, Nat. Chem 6 (2014) 376–377.